Influence of process parameters on energetic properties of sputter-deposited Al/CuO reactive multilayers

Vidushi Singh, Baptiste Julien, Ludovic Salvagnac, Sylvain Pelloquin, Teresa Hungria, Claudie Josse, Mohamed Belhaj, Carole Rossi

Influence of process parameters on energetic properties of sputter-deposited Al/CuO reactive multilayers

Vidushi Singh[1], Baptiste Julien[1], Ludovic Salvagnac[1], Sylvain Pelloquin[1], Teresa Hungria[2], Claudie Josse[2], Mohamed Belhaj[3], Carole Rossi[1]

[1] LAAS-CNRS, University of Toulouse, 7 Avenue du colonel Roche, 31400 Toulouse, France
[2]Centre de Micro Caractérisation Raymond Castaing (UMS 3623), 3 Rue Caroline Aigle, 31400 Toulouse, France
[3]ONERA-DPHY, 2 Avenue Edouard Belin, 31055 Toulouse, France

E-mail: rossi@laas.fr

Received xxxxxx
Accepted for publication xxxxxx
Published xxxxxx

Abstract

In this study we demonstrate the effect of change of the sputtering power and the deposition pressure on the ignition and the combustion properties of Al/CuO reactive thin films. A reduced sputtering power of Al along with the deposition carried out at a higher-pressure result in a high-quality thin film showing a 200% improvement in the burn rate and a 50% drop in the ignition energy. This highlights the direct implication of the change of the process parameters on the responsivity and the reactivity of the reactive film while maintaining the Al and CuO thin-film integrity both crystallographically and chemically. Atomically resolved structural and chemical analyzes enabled us to qualitatively determine how the microstructural differences at the interface (thickness, stress level, delamination at high temperatures and intermixing) facilitate the Al and O migrations and impact the overall nano-thermite reactivity. We found that the deposition of CuO under low pressure produces well-defined and similar Al-CuO and CuO-Al interfaces with the least expected intermixing. Our investigations also showed that the magnitude of residual stress induced during the deposition plays a decisive role in influencing the overall nano-thermite reactivity. Higher is the magnitude of the tensile residual stress induced, stronger is the presence of gaseous oxygen at the interface. By contrast, high compressive interfacial stress aids in preserving the Al atoms for the main reaction while not getting expended in the interface thickening. Overall, this analysis helped in understanding the effect of change of deposition conditions on the reactivity of Al/CuO nanolaminates and several handles that may be pulled to optimize the process better by means of physical engineering of the interfaces.

Keywords: Nanothermite, Al/CuO nanolaminates, sputtering deposition, thin film

1. Introduction

Alumino-thermite materials, also referred to as thermites, represent an interesting class of energetic substances because of their large volumetric energy densities (up to 16 kJ/cm^3), high adiabatic flame temperature (> 2600 °C), and high reaction (burn) rate in the case of nanostructures. These materials undergo a characteristic oxidation-reduction reaction involving Aluminum (Al) and a Metallic Oxide (MO) leading to the formation of a stable product. These energetic nanomaterials are known to have better combustion efficiencies and better ignitability compared to the typical Fulminic acid isomers energetics, represented by a common molecular formula CHNO (including Cyanic acid, Isocyanic acid and Isofulminic acid), and are relatively much safer [1-6]. In general, a reduction in the grain size of Al and metal oxide increases the effective surface area and henceforth reduces the reaction barrier and results in an increased overall homogeneity. Hence, an increased burn rate and ignition response are obtained while maintaining high combustion temperatures. Ever since the discovery of such behavior, different nano-thermites with specific shape (nanowire [7-12], core shell [13], macro-porous structures [14], nanoparticles

mixture [15-17], nano-foils [3, 18-19]) and length scale (tens to few hundreds nm) have been actively investigated for a wide range of applications including actuations [20-22], propellant rate modifiers [12, 23], welding [24-25], biocidal action [26-27], micro initiation and environmentally clean primers [28-31]. These works have experimentally demonstrated that a variety of different combustion effects can be obtained by manipulating the reactive system (Al and oxide) and its interfaces at the nanoscale, which cannot be otherwise achieved in bulk. An interesting approach to create a high density and a high interfacial surface area composite in thermites is by creating laminate structures through Physical Vapor Deposition (PVD). Indeed, thermite nanolaminates offer a highly controllable architecture, and have been incorporated into a variety of micro-pyrotechnic devices commonly used in micro-electromechanical systems (MEMS) [21, 32-37].

From a material point of view, Al/CuO nanolaminates have drawn particular attention due to their low ignition threshold, high reactivity (burn rate up to 100 m/s) and gas generation ability. The effects of different parameters of the layered Al/CuO systems with respect to bilayer thicknesses [2, 38-39], equivalence ratios [40-41], thin insertion layers [42-44], sample width [39, 45], oxidation state of the metal in the oxide layer and additives have been widely studied [46-47]. Decreasing the bilayer thickness has a positive impact on the combustion rates. Replacing alumina interfacial layer between CuO and Al with a ZnO nanolayer leads to a substantial increase in the efficiency of the overall reaction. Incorporating a Cu nanolayer at the interface of the Al/CuO multilayers has been reported to have enabled the reduction of the onset reaction temperature and a better reactivity. Adding additives such as gold nanoparticles [36, 48] or micropores accelerate the combustion rate under certain conditions.

From a technical perspective, the emergence and development of Al/CuO nanolaminates have benefited from the versatile magnetron sputtering technique, which enables a reliable high-quality deposition as well as well-adhered metallic and oxide thin-films. In particular, DC magnetron-sputtering has rapidly developed over the last decade to become a standard manufacturing process for Al/CuO nano-thermites. It offers several advantages: (i) first, it is a simple process that utilizes non-hazardous gases such as argon and oxygen; (ii) second, high purity thin-films are obtained and (iii) third, it offers large-area scalability rendering the technology transfer to the industry a viable process. The sputtering power and the partial pressure of the gas remarkably affect physical properties, material phase and combustion properties of each of the Al and CuO nanolayers. A very recent study [49] showed that varying the vacuum conditions during the deposition of Al nanolayer greatly impact the Al/CuO multilayer self-propagation reaction rates. The authors found that the burn rate decreases with increasing chamber pressure i.e. increasing the quantity of impurities during Al deposition.

In this article, for the purpose of adding new experimental data to Al/CuO sputtered reactive materials family, we study the influence of two parameters: the Al sputtering power and the reactive O_2 mass flow during the CuO deposition, on the multilayer combustion properties. Corresponding to the changes in the process conditions for the nanolayer deposition, three thin film stacks were prepared and their energetic properties compared. We found that for CuO, by controlling the pressure with increased oxygen flow, the burn rate improves by 100%. A reduced sputtering power of Al with the deposition carried out at a higher pressure resulted in a high-quality thin film showing a 200% improvement in the burn rate. A combination of different characterization techniques such as X-Ray diffraction, high resolution transmission electron microscopy and energy loss electron spectroscopy as well as differential scanning calorimetry were used to ascertain the likely cause of the improvement in the combustion properties by changing the process conditions. This technological study found that the residual stress is greatly impacted by the deposition parameters, and affects the reactivity in that a high compressive interfacial stress aids in preserving Al atoms for the main reaction while not getting expended in the interface thickening. Overall, this analysis helps in understanding the effect of change of the deposition conditions on the reactivity of Al/CuO nanolaminates as well as look into physically engineered multilayer stacks for optimizing the process.

2. Materials and Methods

2.1 Preparation of Al/CuO multilayers

Three different tri-layers each sputter-deposited onto a silicon substrate using different process parameters (**Table 1**), were prepared to perform a head-to-head comparison: $Al_{800W}/CuO_{8mTorr}/Al_{800W}$, $Al_{400W}/CuO_{8mTorr}/Al_{400W}$ and $Al_{800W}/CuO_{4mTorr}/Al_{800W}$. The direct current (DC) magnetron sputtering deposition, run in an equipment from TFE (Thin Film Equipment, Italy), began with a 100 nm thick Al layer, followed by a 200 nm thick CuO layer and finally finishing with a 100 nm thick Al layer using Neyco, France purchased 99.99% purity, 20 cm by 8 cm and 6 mm thick Al and Cu targets. The deposition was carried out at room temperature. The chamber is pumped down to a base pressure of about 10^{-7} mTorr before introducing the gases to achieve the desired chamber pressure (also called deposition pressure). For CuO nanolayers, the oxygen and the argon partial pressures were adjusted via percentage flow control with respect to Argon, an equipment inbuilt function. The deposition rate is defined per pass of the substrate holder in front of the target in the horizontal plane (**Figure S1**). The sample is centred at ~ 15 mm from the target as shown in **Figure S1**. The substrate holder is grounded. Further information about the deposition process is available in the **SI**.

Table 1: *Sputtering process parameters for Al and CuO thin-films*

Layer label	Al_{800W}	CuO_{8mTorr}	Al_{400W}	CuO_{4mTorr}
Target	Al	Cu	Al	Cu
Base pressure (mTorr)	10^{-7}	10^{-7}	10^{-7}	10^{-7}

Chamber pressure (mTorr)	4	8	12	4
Ar gas flow (%)	100	100	100	100
O_2 gas flow (%)	0	50	0	80
Power (W)	800	600	400	600
Layer thickness (nm)	100	200	100	200
Deposition rate (/pass)	5.5	3.4	1.4	4.0

In addition to the fabrication of the tri-layer stacks for the structural and the interfacial analysis, devices with 13 bilayers (BL) of each configuration, Al_{800W}/CuO_{8mTorr}, Al_{400W}/CuO_{8mTorr} and Al_{800W}/CuO_{4mTorr}, were fabricated to ascertain the ignition and combustion properties. For combustion tests, lines of nano-thermites with dimensions of 25 mm (length) × 2 mm (width) were sputter-deposited through a patterned shadow mask onto a 32 mm (length) × 18 mm (width) × 500 µm (thick) glass slide and ignited using a resistive heated titanium filament. Prior to the thermite deposition, a photolithography process was used to pattern 300 nm thick Ti resistors on 4-inch glass wafers. Au (800-nm thick) was evaporated onto the surface and then patterned to define the Ti filament and Au electrical pads. A second device, used to carry out the ignition delay measurements, was fabricated following a similar process but using a different shadow mask, with an active thermite area of 5.6 × 6.7 mm^2. Note that for both ignition and combustion tests, the Al/CuO bilayer thickness is chosen to be 300 nm, with Al and CuO layer each being 150 nm thick. This corresponds to an equivalent ratio of 2:1 (fuel-rich configuration), in accordance with previous studies [1, 2].

2.2 Material characterization

The as-deposited and annealed thin-film stacks were characterized by X-Ray Diffraction (XRD) using a Bruker D8 Discover X-Ray Diffractometer to analyze the lattice structure and the phase. A Bragg-Brentano geometry was used to obtain 2θ scans using grazing incidence (GI) where the angle of incidence, ω was kept constant at 0.1°. The measurement was carried out from 20° to 80° with a step size 0.05°. X-Ray Reflectometry (XRR) was used to determine the film density using the same system. The layer thickness and the residual stress (of a nanolayer and a bilayer) were obtained by mechanical profilometry using a KLA Tencor P16+. The thin film residual stress was calculated using **SI**, **Equation S1**, wherein a pre and a post-deposition radius of curvature of the substrate along the same trace was measured using a mechanical profilometer. In each case, the residual stress was measured for one Al/CuO bilayer. The reader may note that Al-CuO refers to CuO deposited over Al while CuO-Al represents Al deposited over CuO.

The morphology and the chemical composition of the multilayers were analyzed by Transmission Electron Microscopy (TEM), Scanning Transmission Electron Microscopy (STEM), Energy Dispersive X-ray Spectroscopy (EDX) and Electron Energy-Loss Spectroscopy (EELS) using a JEOL cold-FEG JEM-ARM200F operated at 200kV equipped with a probe Cs corrector reaching a spatial resolution of 0.078 nm. EDX spectra were recorded on a JEOL CENTURIO SDD detector. EELS data were acquired on a Gatan Imaging Filter Quantum (energy resolution of 0.3 eV) using a dispersion of 0.5 eV/channel, a collection semi angle of 19.4 mradians and a convergence semi-angle of 14.8 mradians. The spatial resolution was estimated at 0.5 nm. FEI Helios NanoLab DualBeam FIB-SEM was used to perform Focused Ion Beam (FIB) technique to prepare the cross-sectional STEM samples.

Additionally, Electron Probe Micro-Analysis (EPMA) was used to quantify the chemical composition of CuO using a Cameca SXFive FE microprobe operated at low voltage (7kV) to have a sub-µm X-ray generation volume. The quantitative analysis was accomplished by comparing the intensities of the characteristic X-rays for elemental Cu and O with the respective intensities for standard natural minerals.

2.3 Characterization of energetic properties

Thermal analysis by Differential Scanning Calorimetry (DSC) was carried out using a NETZSCH DSC 404 F3 Pegasus system. The scan was performed at a constant heating rate of 10 °C.min^{-1} up to 1000 °C under a 50 mL.min^{-1} flow of Ar. The thermograms were normalized to the respective mass of the nano-thermite, typically ~5 mg, and manually baselined. Concerning ignition experiments, test devices were ignited by resistive heating, sending a D.C. current pulse through the Ti filament. The value of the electrical current was adjusted for each test according to the resistor value, in order to work with the same dissipated power (6 W). The ignition delay of the nano-thermite was measured using a photodiode (VISHAY, BPV10) polarized at 5 V placed a few centimetres away from the sample and capable of detecting the optical flash emitted during the ignition event. The photocurrent generated by the diode was measured through a dummy resistance (1 kΩ). All the signals (current, voltage and photodiode signal) were acquired by a digital oscilloscope during each test, and then processed using homemade routines. The experimental setup is presented in **Figure 1a**. For each type of sample, a total of 6 devices were ignited and statistical values are reported. The combustion experiments were performed under the atmosphere using a high-speed imaging setup that included an ultra-fast camera (VEO710, Phantom, USA) capturing the self-propagating reaction with a framerate of 48000 fps and a resolution of 512 × 64 pixels. The imaging setup is presented in **Figure 1b**. The recorded films were then processed and the burn rate was measured for each test. Several combustion tests were performed for each configuration and an average value (and standard deviation) was calculated. Devices from the three configurations (Al_{800W}/CuO_{8mTorr}, Al_{400W}/CuO_{8mTorr} and Al_{800W}/CuO_{4mTorr}) are subjected to the exact same experimental conditions.

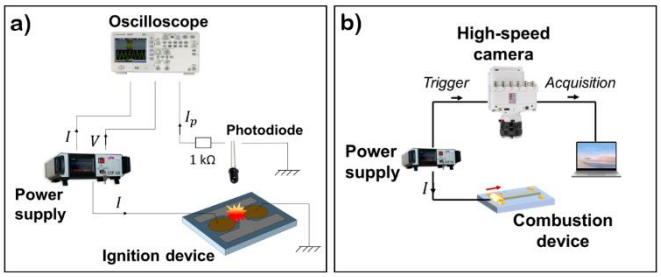

Figure 1: Schematic view of the experimental setup used for **a)** ignition tests and **b)** combustion tests

3. Results and Discussions

3.1 Effect of the sputtering power and gas flow on the physical and chemical characteristics of Al and CuO nanolayers

The deposition process was optimized to obtain high-quality single-phase Al and CuO thin-films. The XRD patterns of the as-deposited Al and CuO nanolayers corresponding to different process conditions **(SI, Figure S2)** clearly show the peaks corresponding to Al and CuO, consistent with COD# 4313214 and COD# 1011148 respectively. The well-defined peaks from planes (1, 1, 1), (2, 0, 0), (2, 2, 0) and (3, 1, 1) corresponding to Al and that (1, 1, 0), (2, 0, 0) and (1, 1, 1) corresponding to CuO corroborate single phase materials. The crystallite size, estimated using the Scherrer equation (**SI, Equation S2**) for Al and CuO layers in the two different respective conditions can be found in **Table 2** with other main physical properties. As for the average grain sizes determined using SEM and shown in **SI, Figure S2**, changing the sputtering power of Al from 800 W to 400W, i.e. reducing the deposition rate to a quarter (**Table 1**), causes the average grain size to decrease from 82 ± 16 nm to 36 ± 7 nm. For the CuO film, decreasing the pressure from 8 mTorr to 4 mTorr does not vary the deposition rate much, and only slightly decreases the average grain size from 38 ± 9 nm to 36 ± 10 nm. In addition, EPMA technique was employed to determine the chemical composition of CuO_{8mTorr} as well as CuO_{4mTorr}, which was found to be ~80% Cu and ~20% O (mass percentages) for the two configurations of the oxides respectively. Modifying the process conditions for the Al metal and CuO deposition does not affect the film crystallinity. Interestingly, lowering the deposition pressure increases the compressive stress in the CuO nanolayer from 42 MPa to 377 MPa, and the roughness goes down by one half to 2.9 nm. The effect of change of sputtering power on the tensile stress in Al nanolayer is not as pronounced, and changes slightly from 20 MPa to 15 MPa. The observed change in the average grain size and henceforth the stress level in the films is consistent with the previous reports [50]. In summary, a decrease in the sputtering power of Al from 800 W in Al_{800W} layer to 400 W in Al_{400W} layer reduces the deposition rate, grain size and the roughness of the Al surface but does not affect the residual stress much. In contrast, a decrease in the gas pressure during CuO deposition from 8 mTorr in CuO_{8mTorr} layer to 4mTorr in CuO_{4mTorr} layer impacts the CuO roughness, which decreases from 4.8 nm to 2.9 nm; as well as the residual stress, which increases from 42 MPa to 377 MPa. It is important to analyze further the impact of process modification on the naturally grown interfacial layer morphology [3-4] as well as, in particular, the residual stress in the bilayers since the effect of interfacial stress is inherently more pronounced in multilayers due to a high interfacial density. Note that the residual stress is also highly related to the nucleation and crystal growth.

Table 2: *Physical properties of as deposited Al and CuO nanolayers*

Property	**Samples/values**			
	Al_{800W}	**CuO_{8mTorr}**	**Al_{400W}**	**CuO_{4mTorr}**
Sputtering conditions	800W, 4mTorr	600W, 8mTorr	400W, 12mTorr	600W, 4mTorr
Average thickness (nm)	100 ± 1	200 ± 1	100 ± 1	200 ± 2
Density ($g.cm^{-3}$) (XRR)	2.7	6.1	2.6	6.1
Cu:O mass ratio		4:1		4:1
Stress [MPa]	20	- 42	15	- 377
RMS Roughness (AFM/XRR) (nm)	2.9	4.8	3	2.9
Crystallite size (Å)	87 ± 1	86 ± 1	87 ± 1	87 ± 1
Average grain size (nm)	82 ± 16	38 ± 9	36 ± 7	36 ± 10

3.2 Effect of the sputtering power and gas flow on the Al-CuO and CuO-Al interface characteristics

Figure 2a-f show the high magnification TEM images from the Al-CuO and CuO-Al interfaces from the three as-deposited configurations, Al_{800W}/CuO_{8mTorr}, Al_{400W}/CuO_{8mTorr} and Al_{800W}/CuO_{4mTorr}. The effect of change of the nanolayer residual stress as a result of the deposition of Al on CuO layer and vice-versa corresponding to different process conditions is summarized in **Table 3**, together with the thickness and some qualitative information about the two interfaces. The interface formed upon the deposition of CuO on Al is thinner and better defined than those formed upon the deposition of Al on CuO, whatsoever be the deposition conditions. This is because of the deposition of CuO on a smooth Al layer whereas the deposition of Al onto a more textured CuO surface induces interfacial damage.

The residual stress analysis showed that the deposition of Al on the highly textured CuO (CuO_{8mTorr}) resulted in a less stressed CuO-Al bilayer (20 MPa and 9 MPa for Al_{800W}/CuO_{8mTorr} and Al_{400W}/CuO_{8mTorr}, respectively) while a more stressed bilayer was obtained with a vice-versa deposition (35 MPa and 47 MPa for Al_{800W}/CuO_{8mTorr} and Al_{400W}/CuO_{8mTorr}). By lowering the oxide deposition pressure

to 4 mTorr, a high compressive stress of 207.4 MPa for CuO_{4mTorr} - Al_{800W} bilayer and 92.3 MPa for Al_{800W}-CuO_{4mTorr} bilayer was observed, inherently pointing out to the higher energy in the system as a whole [51]. Evidently, a decreased CuO surface roughness from 4.8 nm to 2.9 nm does not impact the film density values but has a direct consequence on the CuO stress and further formation of the Al-CuO interfaces.

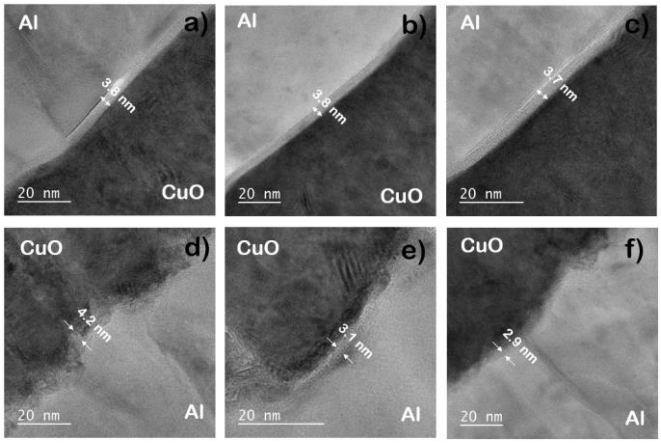

Figure 2: High magnification TEM micrographs of as deposited tri-layers showing Al-CuO interface from: a) Al_{800W}-CuO_{8mTorr}, b) Al_{400W}-CuO_{8mTorr} and c) Al_{800W}-CuO_{4mTorr} and CuO-Al interface from: d) CuO_{8mTorr}-Al_{800W}, e) CuO_{8mTorr}-Al_{400W} and f) CuO_{4mTorr}-Al_{800W}

Table 3: *Residual stress and interface properties of as deposited Al/CuO bilayers having Al-CuO and CuO-Al interfaces*

Bilayer	Average 1 BL thickness (nm)	Residual stress (MPa)	Interface thickness (nm)	Interface quality
Al_{800W}-CuO_{8mTorr}	313 ± 4	35	3.8 ± 0.1	Well-defined, amorphous *(Figure 2a)*
CuO_{8mTorr}-Al_{800W}	304 ± 2	20	4.2 ± 0.7	Ill-defined, non-homogeneous and dense *(Figure 2d)*
Al_{400W}-CuO_{8mTorr}	288 ± 2	47	3.8 ± 0.1	Well-defined, amorphous *(Figure 2b)*
CuO_{8mTorr}-Al_{400W}	286 ± 1	9	3.1 ± 0.8	Ill-defined, non-homogeneous and dense *(Figure 2e)*
Al_{800W}-CuO_{4mTorr}	308 ± 1	-92	3.7 ± 0.1	Well-defined, amorphous *(Figure 2c)*
CuO_{4mTorr}-Al_{800W}	285 ± 1	-207	2.9 ± 0.7	Defined, non-homogeneous, dense (*Figure 2f)*

While the type and the magnitude of residual stress in the bilayers do not affect the thickness of the naturally grown interface, the interfacial quality is its direct consequence (**Table 3**). The presence of compressive stress intrinsically leads to better defined interfaces. Nonetheless, each of the two interfaces, Al-CuO and CuO-Al are fully dense with no signs of delamination and voids.

The stress level, bringing mechanical energy to the system, affects the Al, Cu and O intermixing during the deposition as observed on the chemical composition profile recorded across the bottom (Al-CuO) and the top (CuO-Al) interfaces (**Figure 3**).

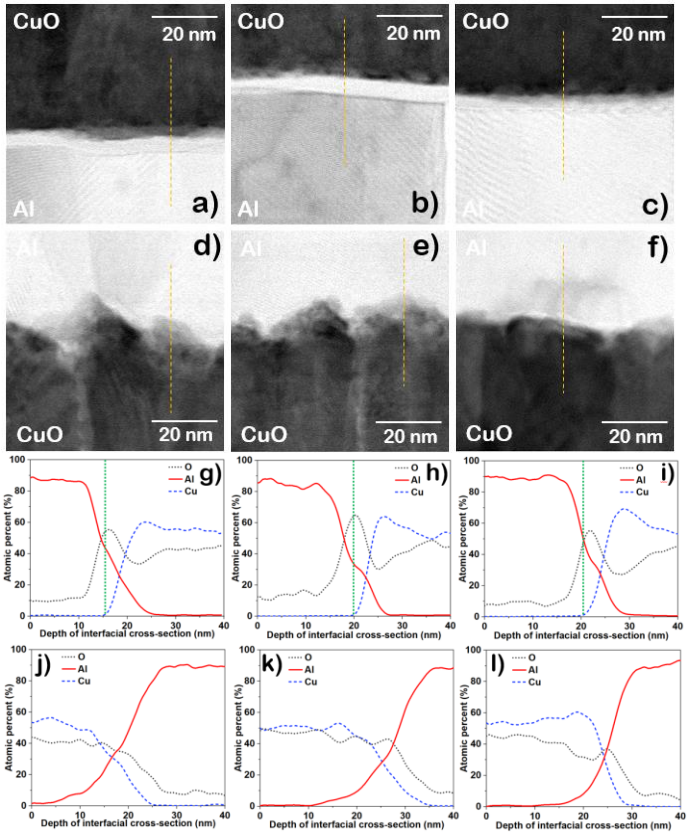

Figure 3: STEM-EDX profile across the top and the bottom interfaces of as deposited multilayers: STEM images (with the line scan indicated) **a)** Al_{800W}-CuO_{8mTorr} **b)** Al_{400W}-CuO_{8mTorr} **c)** Al_{800W}-CuO_{4mTorr}, **d)** CuO_{8mTorr}-Al_{800W} **e)** CuO_{8mTorr}-Al_{400W} (**f)** CuO_{4mTorr}-Al_{800W}, and, the corresponding EDX profiles (**g-l)**

Bottom interface: The Al-CuO interface, obtained upon the deposition of CuO on a smooth Al layer (**Figure 3a-c**), appears to be similarly well-defined across the samples corresponding to the three different process conditions, mainly characterized by the presence of ~4 nm thick amorphous alumina as a result of Al oxidation right before CuO deposition over it. The quantification of the chemical

composition obtained from the EDX profile (**Figure 3g-i**) showed a very clear presence of AlO_x (in the vicinity of the interface, marked by green dotted line in **Figure 3g-i**), and hence some amorphization of the interface is expected as a result of the deposition.

Top interface: Things are more complicated when looking at the bottom interface formed upon the deposition of Al on the relatively more stressed CuO layer (**Figure 3j-l**). The top interface in general was found to be non-homogeneous across the samples corresponding to different process conditions. Whereas the CuO_{8mTorr}-Al_{800W} and CuO_{8mTorr}-Al_{400W} interfaces were highly ill-defined, that of CuO_{4mT}-Al_{800W} was observed to be better defined. No interfacial damage was observed but the top CuO-Al interface was characterized by severe Al, Cu and O intermixing as seen on the EDX line scans obtained across each of the interfaces and shown in **Figure 3j-l.** In the proximity of the CuO_{4mTorr}-Al_{800W} interface, the concentration of Al, Cu and O showed a sharper change (**Figure 3l**), unlike the other two interfaces (CuO_{8mTorr}-Al_{800W} and CuO_{8mTorr}-Al_{400W}), where the change in the concentration profile is gradual and over a relatively larger depth of the interfacial cross section (**Figure 3j-k**). This substantiates the thinner CuO_{4mT}-Al_{800W} interface and suggests lesser interfacial mixing.

3.3 Effect of the sputtering power and the gas flow on the energetic properties of Al and CuO thin-films

The ignition delay, ignition energy and burn rate for each configuration is shown in **Figure 4**. Compared to the Al_{800W}/CuO_{8mTorr} sample with an ignition delay of 0.10 ± 0.041 ms, that for Al_{400W}/CuO_{8mTorr} as well as Al_{800W}/CuO_{4mTorr} improves by at least a 100%, to 0.05 ± 0.025 ms and 0.042 ± 0.01 ms respectively. However, the total spark energy (integral of the photodiode signal) is reduced by one half compared to the Al_{800W}/CuO_{8mTorr} sample. A decrease in the sputtering power of Al layer from 800 W in Al_{800W}/CuO_{8mTorr} sample to 400 W in Al_{400W}/CuO_{8mTorr} brings about a two-times improvement in the burn rate from 7 ± 0.2 m/s to 14 ± 1.6 $m.s^{-1}$. Decreasing the deposition pressure from 8 mTorr in Al_{800W}/CuO_{8mTorr} multilayer to 4 mTorr Al_{800W}/CuO_{4mTorr} increases the burn rate to 12 ± 2.5 $m.s^{-1}$, which is twice the burn rate obtained for the Al_{800W}/CuO_{8mTorr} reactive multilayers.

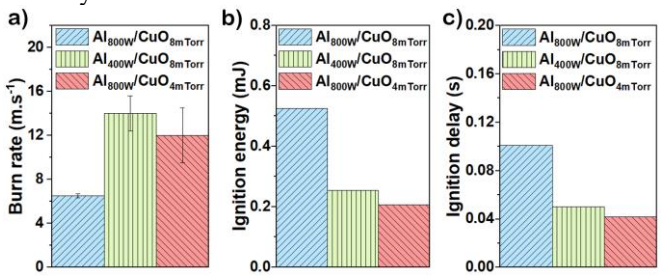

Figure 4: *Combustion properties of 13 BL Al/CuO (150nm/150nm) devices* ***a)*** *Burn rate* ***b)*** *Ignition energy and* ***c)*** *Ignition delay*

Such improvement in the combustion properties cannot only be attributed to the changes in the thermal properties, as Al and CuO nanolayers feature the similar chemical and physical properties, except the residual stress level. This indicates that a change in the process conditions may lead to different reactional pathways such as the ones mediated by the stress. Interestingly, X. Dong et.al. previously concluded in their stress-oxidation coupling study that the tensile stress tends to reduce the energy barrier to oxygen diffusivity while compressive stress increases it. This leads to a reduced oxidation rate in the former as opposed to an enhanced oxidation rate in the latter [52]. In addition, our experimental findings also show that the change in the process conditions for Al and CuO deposition somewhat modifies the average grain size. Therefore, there is a merit in stating that a change in the grain size can affect the combustion properties as well, considering that the grain boundaries can constitute enhanced diffusion paths for both Al and O ions. Indeed, it has been shown previously that for a fixed bulk density of a material (powders), the combustion rate tends to increase with decreasing particle size [53-54].

To observe the nature of the exothermic events and better understand the likely cause in the improvement of the combustion properties by changing the process conditions and therefore nanolayer grain size and stress level, thermal analyses were performed on the Al/CuO multilayers corresponding to the three different configurations of the process conditions. All the samples release heat, as observed in the DSC traces shown in **Figure 5**, with a major exothermic peak rising after 400°C. No major differences are observed; for all the samples, three main exothermic events are detected. A strong exothermal peak corresponding to the main thermite reaction with a peak at 590 °C is recorded followed by a less intense exotherm between 670 °C and 800 °C. A first small broad exotherm event is observed between 400 °C and 500 °C which is a direct consequence of the dual diffusion of Al and O atoms released from CuO through the naturally grown interface into the adjacent layers. This leads to the growth of an Al rich interfacial layer alumina, namely Al_xO_y. The main reaction began just after 500 °C and is characterized by a sharp rise in the exothermal peak intensity. This follows the traditional oxidation reaction reported previously [48]. This event is stopped by the conversion of amorphous alumina to γ-alumina leading to a sharp decrease. The second high-temperature event is simply the continuation of Al oxidation, both in γ-alumina and liquid phase.

While the Al melting is clearly recorded in the Al_{800W}/CuO_{8mTorr} sample (endotherm at ~620°C), the exact temperature of the event is not recorded for the other more reactive samples, featuring a faster burn rate and a lower ignition threshold. The Al + CuO heat of reaction (ΔH_{reac}) generated below 950°C, calculated by integrating the exothermic peaks over time in the temperature range of 20°C to 950°C and normalized with respect to the foil mass, is 1537 J/g, 1989 J/g and 2000 J/g for Al_{800W}/CuO_{8mTorr}, Al_{400W}/CuO_{8mTorr} and Al_{800W}/CuO_{4mTorr} respectively. This is below the theoretical heat of reaction of 3300 J/g for Al:CuO mass ratio of 2:1 (non-stoichiometric condition) [55]. Interestingly, we see the maximum heat of reaction for Al_{800W}/CuO_{4mTorr} multilayer, which also exhibits a relatively

faster burn rate and low ignition energy. Since Al_{800W}/CuO_{4mTorr} and Al_{400W}/CuO_{8mTorr} multilayers samples produce more heat, it is not unexpected that they offer higher combustion rate as well as opposed to Al_{800W}/CuO_{8mTorr} sample.

It is clear that in comparison with the Al_{800W}/CuO_{8mTorr} sample (less reactive), Al_{400W}/CuO_{8mTorr} and Al_{800W}/CuO_{4mTorr} multilayers samples consume Al fuel far more efficiently. Since the magnitude of ΔH_{reac} is proportional to the amount of the specie that react, we see that for the latter two samples, nearly 60% of the available Al is used up in powering the reaction, whereas the former less reactive sample appears to use about 46%. This might be an outcome of more availability of the fuel coming from the fact that less interfacial damage results in a higher oxygen inter-diffusion barrier leading to less consumption of Al during the formation of the interfacial alumina, occurring during the multilayer growth (further discussed in the next section).

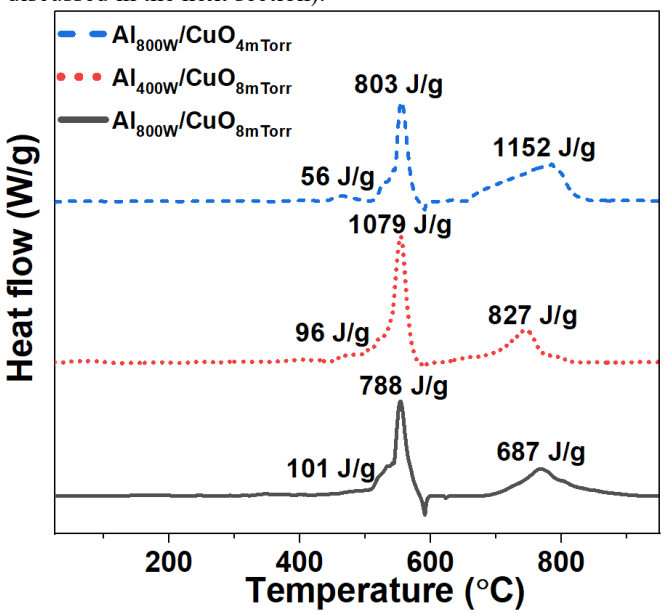

Figure 5: *DSC traces from the as-deposited multilayers: Al_{800W}/CuO_{8mTorr}, Al_{400W}/CuO_{8mTorr} and Al_{800W}/CuO_{4mTorr}*

The heats of reaction corresponding to each exothermic event, including the broad bump prior the reaction onset, as indicated on the DSC trace shown in **Figure 5** provide interesting information as well. The most striking feature about the Al_{800W}/CuO_{8mTorr} sample (less reactive) is that compared to the other two, it offers a lower barrier to Al and oxygen diffusion prior to the reaction onset. This is deduced from the highest heat of reaction (101 $J.g^{-1}$) in Al_{800W}/CuO_{8mTorr} sample compared to that of Al_{400W}/CuO_{8mTorr} (96 $J.g^{-1}$) and Al_{800W}/CuO_{4mTorr} (56 $J.g^{-1}$) observed during the exothermic bump prior to the onset. The Al_{800W}/CuO_{4mTorr} sample characterized by well-defined Al-CuO and CuO-Al interfaces, and staging least interdiffusion between Al, Cu and O contribute to this phenomenon. The heat of reaction corresponding to the main event however does not change as a result of the change in the deposition pressure of CuO from 8 mTorr (788 $J.g^{-1}$) to 4 mTorr (803 $J.g^{-1}$). Whereas for the Al_{400W}/CuO_{8mTorr} multilayer, highest heat of the main reaction is observed to be 1079 $J.g^{-1}$. A greater accessibility to the fuel for the main reaction at low temperature supplements the enhanced intensity of the main exotherm unlike Al_{800W}/CuO_{8mTorr}, wherein a major portion of Al atoms is consumed in enriching the interfacial alumina. The total heat of reaction generated during the last exothermal event is least for less reactive Al_{800W}/CuO_{8mTorr} sample (687 $J.g^{-1}$) compared to the two others. This confirms a lower availability of Al during this event, as it was consumed during the intermixing at lower temperatures (prior to Al melting). In other words, a relatively large amount of Al may have been used up in the thickening of Al_xO_y intermixing at the interfaces which may be correlated to the high tensile stress in CuO_{8mTorr}-Al_{800W} bilayer, favoring Al and O diffusion. By contrast, Al_{800W}/CuO_{4mTorr} multilayer sample, featuring a higher responsivity (lower ignition energy), is characterized by homogeneous, well defined and smooth interfaces, in addition to a high compressive stress that may limit the transport of both Al and oxygen at low temperature.

Overall, the analysis of the exothermal events strongly suggests that the differences in the reactivity seen on the samples corresponding to different process conditions come from the dissimilar participation of Al atoms from the Al reservoir in the formation and further evolution of the interfaces between Al and CuO layers. This questions the role of stress and/or grain size. We suggest that both of these factors may enhance the Al and oxygen transport at low temperatures (< 500 °C) since the onset of the main reaction is directly affected by the thickness and composition of the interfacial layer in terms of Al enrichment. Next, imaging the evolution of the interfacial layer upon annealing with TEM is the most direct way to examine this last conjecture. The target temperature for annealing were set at 400 °C and 500 °C as a result of the DSC traces, wherein the first broad exotherm and the main reaction onset are observed just after 400 °C and after 500 °C, respectively.

3.4 Al_xO_y interface evolution upon annealing

Figure 6a-c show the high magnification TEM micrographs from the top and bottom Al-CuO interfaces post the annealing treatment. Compared to the Al_{800W}/CuO_{8mTorr}, less reactive sample, where severe delamination is observed at both top and bottom interfaces, Al_{400W}/CuO_{8mTorr}, the most reactive sample i.e. the one demonstrating the highest burn rate, shows delamination only at the top interface (**Figure 6**). So, a comparable tensile stress level prior to annealing (~30 and ~25 MPa) in both the bilayers (Al_{800W}-CuO_{8mTorr} and CuO_{8mTorr}-Al_{800W}) justifies the post anneal damage in Al_{800W}/CuO_{8mTorr}. For Al_{400W}/CuO_{8mTorr}, the pre-anneal residual stress in Al_{400W}-CuO_{8mTorr} bilayer is observed to be high, ~47 MPa against only few megapascals in CuO_{8mTorr}-Al_{400W} bilayer (**Table 2**). This plausibly explains the delamination observed only at the bottom Al-CuO interface post anneal. Interestingly, Al_{800W}/CuO_{4mTorr} multilayer did not show any delamination at both the interfaces. This is despite the fact that the CuO_{4mTorr}-

Al_{800W} bilayer is characterized by a very high compressive residual stress prior to annealing in addition to exhibiting relatively defined and uniform interfaces. The compressive stress does not mechanically alter the innate nature of the interface in that no damages were seen post-anneal. Additionally, an Al recrystallization step is observed at this temperature consistent with the previous reports [56]. Compared to the film subjected to annealing at lower temperature (400°C), the CuO film annealed at 500°C possess a more granular structure as opposed to a columnar structure. Furthermore, there is a reduction in the layer thickness observed post anneal, as well as the thickening of the interfaces as shown in **Figure 6**. We observe that the thickness of the top CuO-Al interfaces increases at a faster rate than the bottom Al-CuO interfaces (**SI, Figure S6**). This is expected given that CuO-Al interface sustains more damage typically due to Al deposition over highly textured CuO. Interestingly, the interface growth is enhanced when the pre-anneal residual stress is high, i.e. > 10 MPa. This is especially visible after annealing at 500 °C and directly impacts the Al reservoir just prior to the reaction onset. Notably, in the case of Al_{800W}/CuO_{8mTorr}, where the outward migration of Al and O is favored due to a higher tensile stress, the thickness of the bottom and the top Al layer are reduced by 7% and 12% respectively. The sample, Al_{800W}/CuO_{4mTorr}, corresponding to the most-defined interfaces pre and post anneal, and characterized by a very high compressive stress interestingly loses a mere 2% (Al-CuO) and 0.5% (CuO-Al) in the Al nanolayer thickness, upholding the tensile stress-mediated reaction pathway.

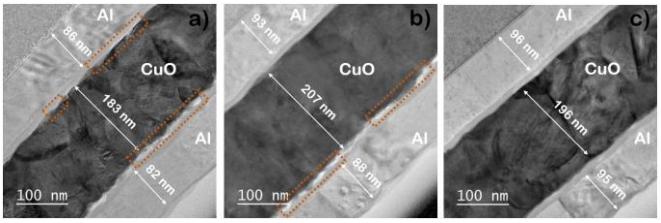

Figure 6: *High magnification TEM micrographs of multilayers annealed at 500°C: a) Al_{800W}/CuO_{8mTorr}, b) Al_{400W}/CuO_{8mTorr} and c) Al_{800W}/CuO_{4mTorr}*

As a final experiment, STEM-HAADF and STEM-EELS were performed on both the top and the bottom interfaces after annealing with the goal to determine the evolution of the oxidation state of Al and Cu. Hence, electron loss near edge structure (ELNES) of Cu $L_{2,3}$-edges at 931-951 eV, O K-edge at 536 eV and Al K edges at 1560 eV were acquired on different zones near and across Al-CuO and CuO-Al interfaces. EELS core loss edges were background subtracted using a power law fit before being plotted. ELNES of the Al and Cu in all the samples annealed at 500°C are shown in **Figure 7a-c**.

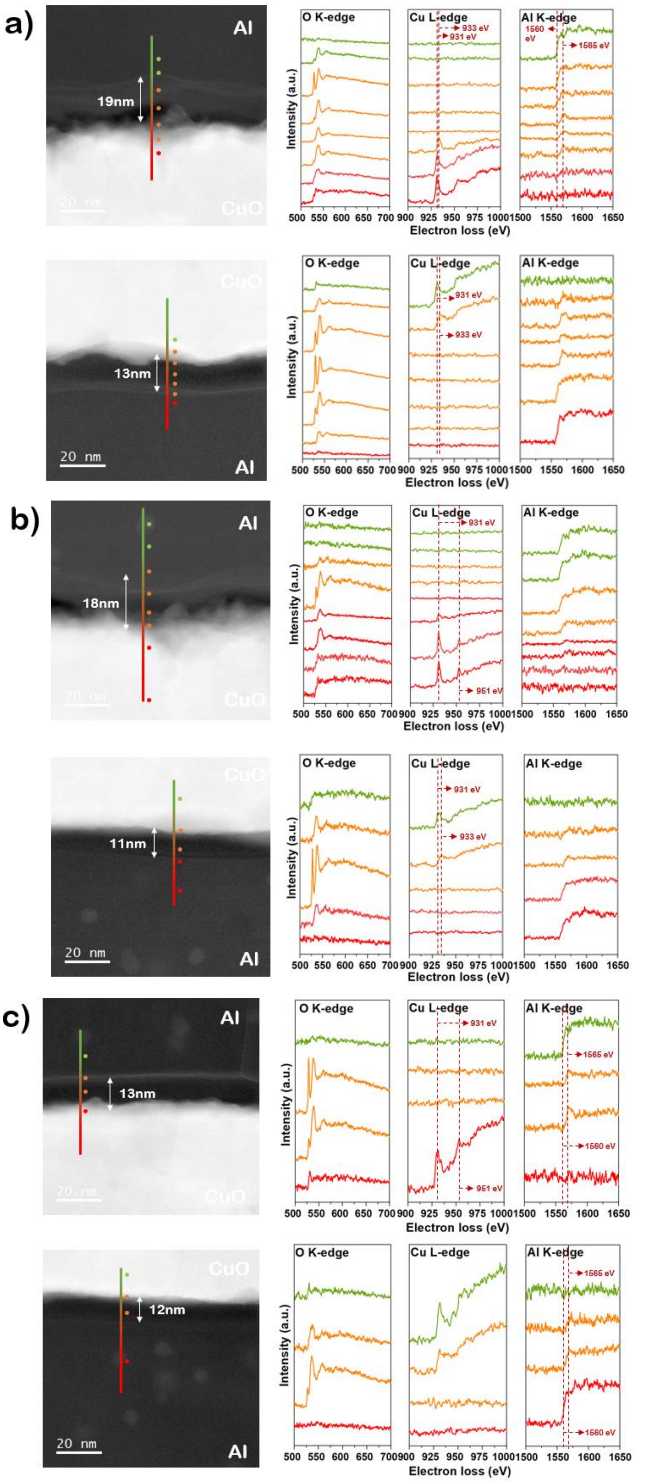

Figure 7: High magnification *STEM-HAADF-EELS of multilayers annealed at 500°C showing O K-edge, Cu $L_{2,3}$ edges and Al K-edge: a) Al_{800W}/CuO_{8mTorr}, b) Al_{400W}/CuO_{8mTorr} and c) Al_{800W}/CuO_{4mTorr}*

Each spectral scan corresponds to a point on the colored line corresponding to that specific region along the interface. The characteristic Cu $L_{2,3}$ ELNES edges at 931 eV and 951 eV corresponding to the $2p_{1/2}$ and $2p_{3/2}$ transitions respectively are

in excellent agreement with previous reports [57-58]. The $2p_{1/2}$ edge is half the intensity of the $2p_{3/2}$ edge analogous to formerly reported literature [48]. The characteristic O-K edge ELNES is observed at about 536 eV consistent with previous observations [59]. In addition, a pre-peak at 529 eV corresponding to the transition from O 1s core is observed at the interface. This might be due to the presence of molecular oxygen that is released as a result of CuO decomposition and has been observed in other experimental studies as well [48, 57-59]. The characteristic Al K edge ELNES is observed at 1560 eV.

The top and bottom interfaces reveal the presence of gaseous oxygen in remarkably similar manner, except the CuO-Al interface thickened faster than Al-CuO interface owing to the effect of surface roughness on the deposition. For the Al_{800W}/CuO_{8mTorr} sample, the severely damaged interfaces aid the outward movement of this oxygen contributing to Al, Cu and O intermixing. This is clear from the high energy shift in Cu L_2 edge to 933 eV, a characteristic of CuO decomposition reaction ($CuO = Cu_2O + ½ O_2$) as shown in **Figure 7a** [58-59]. A shift in Al K edge to 1565 eV is seen as we move along the interface from Al to CuO. This shift corresponds to an increase in oxidation state of Al from 0 to +3. This observation corroborates the formation of amorphous alumina responsible for the reservoir consumption as discussed above.

In contrast, Al_{400W}/CuO_{8mTorr}, the most reactive sample, featuring interfacial delamination and higher tensile stress in the CuO-Al bilayer is also characterized by a weaker molecular oxygen pre-peak at 529 eV. Whereas the lowly stressed Al-CuO bilayer shows much more pronounced presence of oxygen liberated at the interface due to the CuO decomposition. The shift of Cu L_2 edge to 933 eV supports such decomposition reaction as well as shown in **Figure 7b**. Interestingly, the trend changes as a result of change of the oxide nanolayer process conditions for the Al_{800W}/CuO_{4mTorr} sample, featuring a high compressive stress in the bilayer. An intense oxygen pre-edge peak is seen at 529 eV only at the CuO-Al interface (**Figure 7c**) whereas there is no such signal at the Al-CuO interface. The reader may recall that this samples also feature the highest heat of reaction and hence a higher burn rate. At sites away from the interface, the O K pre-edge peak as well as the shift in Al K edge towards higher energy losses are not observed. Based on this, it can be concluded that the oxygen liberated because of CuO decomposition (dominant at higher temperature) is primarily consumed in the thickening of the alumina layer and intermixing. With that being the case, it could be less likely for this gaseous oxygen to cause mechanical failure in the devices since the phenomenon is limited to the interface only. Both the microstructural damages at the interfaces and the magnitude of the residual stress in the Al/CuO bilayers control the reactivity by affecting the diffusivity of aluminum and oxygen, and hence the consumption of Al atoms (higher the magnitude, stronger is the presence of gaseous oxygen). Conspicuously, a high compressive stress aids in preserving the Al atoms for the main reaction while not getting expended in the interface thickening.

4. Conclusion

We studied the effect of varying sputtering process conditions in terms of power density and deposition pressure, on the Al/CuO nano-thermite films by means of preserving the stoichiometry and using no chemical modifications in the nanolayers' stack. The difference in the responsivity and the reactivity of Al_{800W}/CuO_{8mTorr}, Al_{400W}/CuO_{8mTorr} and Al_{800W}/CuO_{4mTorr} multilayer samples appear to come from the stress-mediated reaction pathway and the microstructural differences at the bottom Al-CuO and the top CuO-Al interfaces. Severe interfacial mixing of Al, Cu and O is found at both interfaces; however, the CuO-Al interfaces are inherently thicker than the Al-CuO interfaces. Compared to the better-defined and homogeneous interfaces of Al_{800W}/CuO_{4mTorr}, Al_{800W}/CuO_{8mTorr} and Al_{400W}/CuO_{8mTorr} exhibit critical interfacial mixing at the CuO-Al interfaces. Post anneal, this proves to be an ineffective barrier against the diffusion of oxygen that consumes a part of the Al reservoir, especially in Al_{800W}/CuO_{8mTorr}, where both interfaces are severely damaged. This study also showed that the residual stress can control the reactivity in that a high compressive stress aids in preserving the Al atoms for the main reaction while not getting exhausted in the interface thickening.

Overall, this study adds to the experimental data of Al/CuO nano-thermite thin-films towards a better understanding of the interfaces as a result of the physical modifications and can serve as one of the basis of advanced interface engineering.

Acknowledgements

The authors acknowledge the support from the European Research Council (ERC) (H2020 Excellent Science) Researcher Award (grant 832889—PyroSafe). This work was also supported by the LAAS-CNRS technology platform, a member of the Renatech network.

Competing financial interests

The authors declare no competing financial interests.

Data availability statement

All data that support the findings of this study are included within the article (and any supplementary files).

References

[1] Zaky, M. G.; Abdalla, A. M.; Sahu, R. P.; Puri, I. K.; Radwan, M.; Elbasuney, S., Nanothermite colloids: A new prospective for enhanced performance. Def Technol 2019, 15 (3), 319-325

[2] Xu, J. B.; Shen, Y.; Wang, C. G.; Dai, J.; Tai, Y.; Ye, Y. H.; Shen, R. Q.; Wang, H. Y.; Zachariah, M. R., Controlling the energetic characteristics of micro energy storage device by in situ deposition Al/MoO3 nanolaminates with varying internal structure. Chem Eng J 2019, 373, 345-354

[3] Rossi, C., Engineering of Al/CuO Reactive Multilayer Thin Films for Tunable Initiation and

Actuation. Propellants, Explosives, Pyrotechnics 2019, 44 (1), 94-108
[4] Hastings, D. L.; Schoenitz, M.; Dreizin, E. L., High density reactive composite powders. J Alloy Compd 2018, 735, 1863-1870
[5] Wu, T.; Lahiner, G.; Tenailleau, C.; Reig, B.; Hungria, T.; Esteve, A.; Rossi, C., Unexpected Enhanced Reactivity of Aluminized Nanothermites by Accelerated Aging. Chem Eng J 2021, 129432
[6] Zhou, X.; Torabi, M.; Lu, J.; Shen, R. Q.; Zhang, K. L., Nanostructured Energetic Composites: Synthesis, Ignition/Combustion Modeling, and Applications. Acs Appl Mater Inter 2014, 6 (5), 3058-3074
[7] Ohkura, Y.; Liu, S. Y.; Rao, P. M.; Zheng, X. L., Synthesis and ignition of energetic CuO/Al core/shell nanowires. P Combust Inst 2011, 33, 1909-1915
[8] Petrantoni, M.; Rossi, C.; Conedera, V.; Bourrier, D.; Alphonse, P.; Tenailleau, C., Synthesis process of nanowired Al/CuO thermite. J Phys Chem Solids 2010, 71 (2), 80-83
[9] Zhang, K.; Rossi, C.; Tenailleau, C.; Conedera, V., CuO Nanowires Grown from Cu Film Heated Under a N-2/O-2 Flow. J Nanosci Nanotechno 2009, 9 (2), 1418-1422
[10] Zhang, K. L.; Rossi, C.; Tenailleau, C.; Alphonse, P.; Chane-Ching, J. Y., Synthesis of large-area and aligned copper oxide nanowires from copper thin film on silicon substrate. Nanotechnology 2007, 18 (27). 29
[11] Yang, Y.; Wang, P. P.; Zhang, Z. C.; Liu, H. L.; Zhang, J. C.; Zhuang, J.; Wang, X., Nanowire Membrane-based Nanothermite: towards Processable and Tunable Interfacial Diffusion for Solid State Reactions. Sci Rep-Uk 2013, 3.
[12] Sabourin, J. L.; Yetter, R. A.; Asay, B. W.; Lloyd, J. M.; Sanders, V. E.; Risha, G. A.; Son, S. F., Effect of Nano-Aluminum and Fumed Silica Particles on Deflagration and Detonation of Nitromethane. Propell Explos Pyrot 2009, 34 (5), 385-393
[13] Zhang, Y. Q.; Sui, H. T.; Li, Y. N.; Wen, J. Z., Energetic characteristics of the Al/CuO core-shell composite micro-particles fabricated as spherical colloids. Thermochim Acta 2020, 689.
[14] Zheng, G. Q.; Zhang, W. C.; Xu, X.; Shen, R. Q.; Deng, J. P.; Ye, Y. H., Preparation of Porous Core/Shell Structure Fe2O3/Al Nanothermite Membrane by Template Method. J Inorg Mater 2015, 30 (6), 610-614.
[15] Nellums, R. R.; Terry, B. C.; Tappan, B. C.; Son, S. F.; Groven, L. J., Effect of Solids Loading on Resonant Mixed Al-Bi2O3 Nanothermite Powders. Propell Explos Pyrot 2013, 38 (5), 605-610.
[16] Pantoya, M. L.; Granier, J. J., Combustion behavior of highly energetic thermites: Nano versus micron composites. Propell Explos Pyrot 2005, 30 (1), 53-62.
[17] Malchi, J. Y.; Foley, T. J.; Yetter, R. A., Electrostatically Self-Assembled Nanocomposite Reactive Microspheres. Acs Appl Mater Inter 2009, 1 (11), 2420-2423.
[18] Xu, J. B.; Tai, Y.; Shena, Y.; Dai, J.; Xu, W.; Ye, Y. H.; Shen, R. Q.; Hu, Y., Characteristics of energetic semiconductor bridge initiator based on different stoichiometric ratios of Al/MoO3 reactive multilayer films under capacitor discharge conditions. Sensor Actuat a-Phys 2019, 296, 241-248.
[19] Mily, E. J.; Oni, A.; LeBeau, J. M.; Liu, Y.; Brown-Shaklee, H. J.; Ihlefeld, J. F.; Maria, J. P., The role of terminal oxide structure and properties in nanothermite reactions. Thin Solid Films 2014, 562, 405-410.
[20] Fleck, T. J.; Ramachandran, R.; Murray, A. K.; Novotny, W. A.; Chiu, G. T. C.; Gunduz, I. E.; Son, S. F.; Rhoads, J. F., Controlled Substrate Destruction Using Nanothermite. Propell Explos Pyrot 2017, 42 (6), 579-584.
[21] Pandey, S. S.; Mastrangelo, C. H., An Exothermal Energy Release Layer for Microchip Transience. 2013 Ieee Sensors 2013, 1759-1762.
[22] Nicollet, A.; Salvagnac, L.; Baijot, V.; Estève, A.; Rossi, C., Fast circuit breaker based on integration of Al/CuO nanothermites. Sensors and Actuators A: Physical 2018, 273, 249-255.
[23] Bezmelnitsyn, A.; Thiruvengadathan, R.; Barizuddin, S.; Tappmeyer, D.; Apperson, S.; Gangopadhyay, K.; Gangopadhyay, S.; Redner, P.; Donadio, M.; Kapoor, D.; Nicolich, S., Modified Nanoenergetic Composites with Tunable Combustion Characteristics for Propellant Applications. Propell Explos Pyrot 2010, 35 (4), 384-394.
[24] Kinsey, A. H.; Slusarski, K.; Sosa, S.; Weihs, T. P., Gas Suppression via Copper Interlayers in Magnetron Sputtered Al-Cu2O Multilayers. Acs Appl Mater Inter 2017, 9 (26), 22026-22036.
[25] Sui, H. T.; Huda, N.; Shen, Z. K.; Wen, J. Z., Al-NiO energetic composites as heat source for joining silicon wafer. J Mater Process Tech 2020, 279.
[26] Feng, J. Y.; Jian, G. Q.; Liu, Q.; Zachariah, M. R., Passivated Iodine Pentoxide Oxidizer for Potential Biocidal Nanoenergetic Applications. Acs Appl Mater Inter 2013, 5 (18), 8875-8880.
[27] Wang, H.; Jian, G.; Zhou, W.; DeLisio, J. B.; Lee, V. T.; Zachariah, M. R., Metal Iodate-Based Energetic Composites and Their Combustion and Biocidal Performance. Acs Appl Mater Inter 2015, 7 (31), 17363-17370.
[28] Dai, J.; Wang, C. G.; Wang, Y. T.; Xu, W.; Xu, J. B.; Shen, Y.; Zhang, W.; Ye, Y. H.; Shen, R. Q., From nanoparticles to on-chip 3D nanothermite: electrospray deposition of reactive Al/CuO@NC onto semiconductor bridge and its application for rapid ignition. Nanotechnology 2020, 31 (19).

[29] Zhu, P.; Shen, R. Q.; Ye, Y. H.; Zhou, X.; Hu, Y.; Wu, L. Z., Energetic Igniters Based on Al/CuO/B/Ti Reactive Multilayer Films. Theory and Practice of Energetic Materials (Vol Ix), Proceedings of the 2011 International Autumn Seminar on Propellants, Explosives and Pyrotechnics 2011, 756-760.
[30] Glavier, L.; Nicollet, A.; Jouot, F.; Martin, B.; Barberon, J.; Renaud, L.; Rossi, C., Nanothermite/RDX-Based Miniature Device for Impact Ignition of High Explosives. Propell Explos Pyrot 2017, 42 (3), 307-316.
[31] Salvagnac, L.; Assie-Souleille, S.; Rossi, C., Layered Al/CuO Thin Films for Tunable Ignition and Actuations. Nanomaterials (Basel) 2020, 10 (10).
[32] Pouchairet, J. L.; Rossi, C., PyroMEMS as Future Technological Building Blocks for Advanced Microenergetic Systems. Micromachines (Basel) 2021, 12 (2).
[33] Larangot B., Conedera V., Dureuil P., Do Conto T., Rossi C. Solid propellant microthruster: An alternative propulsion device for nanosatellite; Proceedings of the 2002 Aerospace Energetic Equipment Conference; Avignon, France. 3–5 July 2019.
[34] Zhu, P.; Hou, G.; Wang, H. Y.; Xu, C.; Zhao, S. F.; Shen, R. Q., Design, Preparation, and Performance of a Planar Ignitor Inserted With PyroMEMS Safe and Arm Device. J Microelectromech S 2018, 27 (6), 1186-1192.
[35] Ervin, M. H., Factors Affecting Substrate Heating with Printed Thermites. Propell Explos Pyrot 2021, 46 (12), 1772-1783.
[36] Julien, B.; Wang, H.; Tichtchenko, E.; Pelloquin, S.; Esteve, A.; Zachariah, M. R.; Rossi, C., Elucidating the dominant mechanisms in burn rate increase of thermite nanolaminates incorporating nanoparticle inclusions. Nanotechnology 2021.
[37] Korampally, M.; Apperson, S. J.; Staley, C. S.; Castorena, J. A.; Thiruvengadathan, R.; Gangopadhyay, K.; Mohan, R. R.; Ghosh, A.; Polo-Parada, L.; Gangopadhyay, S., Transient pressure mediated intranuclear delivery of FITC-Dextran into chicken cardiomyocytes by MEMS-based nanothermite reaction actuator. Sensor Actuat B-Chem 2012, 171, 1292-1296.
[38] Lahiner, G.; Nicollet, A.; Zapata, J.; Marín, L.; Richard, N.; Djafari-Rouhani, M.; Rossi, C.; Estève, A., A diffusion–reaction scheme for modeling ignition and self-propagating reactions in Al/CuO multilayered thin films J Appl Phys 2017, 122 (15).
[39] Tai, Y.; Xu, J. B.; Wang, F.; Dai, J.; Zhang, W.; Ye, Y. H.; Shen, R. Q., Experimental and modeling investigation on the self-propagating combustion behavior of Al-MoO3 reactive multilayer films. J Appl Phys 2018, 123 (23).
[40] Bahrami, M.; Taton, G.; Conedera, V.; Salvagnac, L.; Tenailleau, C.; Alphonse, P.; Rossi, C., Magnetron Sputtered Al-CuO Nanolaminates: Effect of Stoichiometry and Layers Thickness on Energy Release and Burning Rate. Propell Explos Pyrot 2014, 39 (3), 365-373.
[41] Wang, H. Y.; Julien, B.; Kline, D. J.; Alibay, Z.; Rehwoldt, M. C.; Rossi, C.; Zachariah, M. R., Probing the Reaction Zone of Nanolaminates at similar to mu s Time and similar to mu m Spatial Resolution. J Phys Chem C 2020, 124 (25), 13679-13687.
[42] Marin, L.; Gao, Y. Z.; Vallet, M.; Abdallah, I.; Warot-Fonrose, B.; Tenailleau, C.; Lucero, A. T.; Kim, J.; Esteve, A.; Chabal, Y. J.; Rossi, C., Performance Enhancement via Incorporation of ZnO Nanolayers in Energetic Al/CuO Multilayers. Langmuir 2017, 33 (41), 11086-11093.
[43] Marin, L.; Nanayakkara, C. E.; Veyan, J. F.; Warot-Fonrose, B.; Joulie, S.; Esteve, A.; Tenailleau, C.; Chabal, Y. J.; Rossi, C., Enhancing the Reactivity of Al/CuO Nanolaminates by Cu Incorporation at the Interfaces. Acs Appl Mater Inter 2015, 7 (22), 11713-11718.
[44] Chen, Y. J.; Ren, W.; Zheng, Z. L.; Wu, G. G.; Hu, B.; Chen, J. H.; Wang, J. X.; Yu, C. P.; Ma, K. F.; Zhou, X. L.; Zhang, W. C., Reactivity adjustment from the contact extent between CuO and Al phases in nanothermites. Chem Eng J 2020, 402, 9.
[45] Xu, J. B.; Tai, Y.; Ru, C. B.; Dai, J.; Shen, Y.; Ye, Y. H.; Shen, R. Q.; Fu, S., Characteristic of energetic semiconductor bridge based on Al/MoOx energetic multilayer nanofilms with different modulation periods. J Appl Phys 2017, 121 (11).
[46] Blobaum, K. J.; Wagner, A. J.; Plitzko, J. M.; Van Heerden, D.; Fairbrother, D. H.; Weihs, T. P., Investigating the reaction path and growth kinetics in CuOx/Al multilayer foils. J Appl Phys 2003, 94 (5), 2923-2929.
[47] Blobaum, K. J.; Reiss, M. E.; Lawrence, J. M. P.; Weihs, T. P., Deposition and characterization of a self-propagating CuOx/Al thermite reaction in a multilayer foil geometry. J Appl Phys 2003, 94 (5), 2915-2922.
[48] Julien, B.; Cure, J.; Salvagnac, L.; Josse, C.; Esteve, A.; Rossi, C., Integration of Gold Nanoparticles to Modulate the Ignitability of Nanothermite Films. Acs Appl Nano Mater 2020, 3 (3), 2562-2572.
[49] Dulmaa, A.; Depla, D., Influence of Impurities on the Front Velocity of Sputter Deposited Al/CuO Thermite Multilayers. Materials 2021, 14 (23)
[50] Lee, H. C., Kim, K., Han, S. Y., Choi, S. K., Lee, E., Jo, M., Yoo, M. S., & Cho, K., Highly Conductive Flexible Metal–Ceramic Nanolaminate Electrode for High-Performance Soft Electronics. ACS Applied Materials & Interfaces 2018, 11(2), 2211–2217
[51] Abadias, G., Chason, E., Keckes, J., Sebastiani, M., Thompson, G. B., Barthel, E., Doll, G. L., Murray, C. E., Stoessel, C. H., & Martinu, L., Review Article: Stress in thin films and coatings: Current status, challenges, and prospects. Journal of Vacuum

Science & Technology A: Vacuum, Surfaces, and Films 2018, 36(2), 020801
[52] Dong, X., Fang, X., Feng, X., & Hwang, K. C., Diffusion and Stress Coupling Effect during Oxidation at High Temperature. Journal of the American Ceramic Society 2012, 96(1), 44–46.
[53] Castells, B., Amez, I., Medic, L., & García Torrent, J., Particle Size Influence on the Transport Classification Labels and Other Flammability Characteristics of Powders. Applied Sciences 2020, 10(23), 8601.
[54] Balakir, A., Bushuev, Y. G., Bareskov, N. A., Kosyakin, A. E., Kudryavtsev, Y. V., & Fedorova, O. N., Rate of combustion of exothermal mixtures. Combustion, Explosion, and Shock Waves 1976, 11(1), 36–38
[55] Zapata, J., Nicollet, A., Julien, B., Lahiner, G., Estève, A., Rossi, C., Self-propagating combustion of sputter-deposited Al/CuO nanolaminates. Combustion and Flame 2019, 205, 389-396
[56] Abdallah, I., Zapata, J., Lahiner, G., Warot-Fonrose, B., Cure, J., Chabal, Y., Esteve, A., & Rossi, C., Structure and Chemical Characterization at the Atomic Level of Reactions in Al/CuO Multilayers. ACS Applied Energy Materials 2018, 1(4), 1762–1770
[57] Leapman, R. D., Grunes, L. A., & Fejes, P. L., Study of theL23edges in the3dtransition metals and their oxides by electron-energy-loss spectroscopy with comparisons to theory. Physical Review B 1982, 26(2), 614–635
[58] Wang, Y., Lany, S., Ghanbaja, J., Fagot-Revurat, Y., Chen, Y. P., Soldera, F., Horwat, D., Mücklich, F., & Pierson, J. F., Electronic structures ofCu2O,Cu4O3, and CuO: A joint experimental and theoretical study. Physical Review B 2016, 94(24)
[59] Jiang, N., & Spence, J. C., Interpretation of Oxygen K pre-edge peak in complex oxides. Ultramicroscopy 2006, 106(3), 215–219